

## INTENSIFICATION OF YEAST BIOMASS CULTURING IN A FILM BIOREACTOR

N.A. Voinov, O.P. Zhukova, and A.N. Nikolaev

Siberian State Technological University,  
pr. Mira 82, Krasnoyarsk, 660049 Russia,  
phone/fax: 391-227-34-53, e-mail: Voynov@Siberianet.ru

Received March 5, 2013; accepted in revised form April 27, 2013

**Abstract:** The results of Doctor N.A. Voinov and his colleagues' research aimed at developing gas-liquid film bioreactors are systematized. Fluid dynamics and heat and mass transfer in a liquid film flowing by gravity down a surface with artificial large-scale roughness have been investigated. Relationships based on the plug flow model are suggested for calculating mass transfer in the working zones of the bioreactor. Ways of raising the productivity of the apparatus and reducing the cost of culturing *Candida scottii* yeast are considered. Closed-loop gas circuit schemes are suggested for the film bioreactor.

**Key words:** film bioreactor, yeast biomass, heat transfer, mass transfer, artificial roughness

UDC 663.12:57.083.13  
DOI 10.12737/2057

### INTRODUCTION

Gas-liquid bioreactors are widely used in the food and related industries, including the production of enzyme preparations, baker's yeast, biopolymers, and other microbiological synthesis products. One of the serious drawbacks of the existing industrial bioreactors is their low biomass output capacity, high stirring and concentrating costs, and large mounts of microbiological synthesis products discharged into the environment because of the low intensity of heat transfer. This imposes limits on the composition of the gaseous substrate, generates temperature distribution nonuniformities in the culture liquid, and does not ensure proper purification of the exit gas from metabolism products.

Of the wide variety of the existing fermenters, the most widely employed ones are bubblers with mechanical stirring and liquid circulation in the working space of the apparatus. However, the energy consumption per unit weight of the resulting biomass in stirred bioreactors is higher than in the other types of apparatuses [1] and is 3–4 (kW h)/kg at a comparatively low biomass concentration (Table 1). Although the stirring of the liquid increases the interfacial area owing to the breakup of gas bubbles, the liquid flow remains mainly laminar and the energy consumed does not afford an adequate increase in the rate of oxygen transport in the liquid phase. In addition, heat removal from the reaction zone of the apparatuses is slow and, as a consequence, the culturing process often takes place at a non-optimal temperature.

One way of increasing the output capacity of the gas-liquid bioreactor is by saturating the culture liquid with the gas in a turbulent liquid film. [2–4] flowing down the surface of contact devices. This technique has found application in microorganism culturing methods developed by the authors [5–10].

**Table 1.** Characteristics of bioreactors

Characteristic	Gas-lift bioreactor	Stirred gas-lift bioreactor	Bioreactor with a suction stirrer	Jet-stirred bioreactor	Film bioreactor
Oxygen transport rate, kg/(m <sup>2</sup> h)	1.1–4.0	4–7	7	0.4–0.7	10
Bulk mass transfer coefficient, h <sup>-1</sup>	200–450	450–1000	1000	100–150	1500–4000*
Surface mass transfer coefficient, m/s	(1.3–5) · 10 <sup>-4</sup>	(5–6) · 10 <sup>-4</sup>	6 · 10 <sup>-4</sup>	(0.4–0.7) · 10 <sup>-4</sup>	(2–5)* · 10 <sup>-2</sup>
Concentration of reducing substances, kg/m <sup>3</sup>	8–30	30	30	8	100
Specific air consumption, m <sup>3</sup> /kg	30–50	34	29–43	10	0–10
Biomass concentration (ADW), kg/m <sup>3</sup>	4–10.5	10	10	4	40–80**
Filling factor	0.33	0.7	0.4	0.33	0.8
Specific energy consumption, kW h/kg	0.8–1.75	2–3	3–4	0.4–0.5	0.6–1.4

\*In the falling liquid film. \*\*Calculated value.

The introduction of a falling-film section for gas absorption in the culture liquid into the stirred apparatus makes it possible to significantly intensify heat and mass transfer and to reduce specific expenses.

Film bioreactors are next-generation apparatuses, and their introduction into industry is impeded by the poor understanding of the heat transfer processes occur-

ring there. The oxygen transfer rate in the falling liquid film can reach  $10 \text{ kg}/(\text{m}^3 \text{ h})$  or over [11], and the surface mass transfer coefficient can be up to  $(2-5) \cdot 10^{-2} \text{ m/s}$ , one order of magnitude larger than in the other types of fermenters. Heat transfer in a turbulent film [12] is also more intensive than in bubble and gas-lift apparatuses. Furthermore, biomass growth in film bioreactors can be carried out without employing mechanical devices for transporting the components of the gaseous substrate, since the gas is uninvolved in the generation of the phase contact surface and in liquid turbulization. Owing to the high rates of oxygen supply and metabolite removal, film bioreactors are capable of processing concentrated nutrient media, ensure a high product output rate and fine purification of the spent gas from metabolites and substrate drops, maintain a high degree of sterility in the process,

and make it possible to organize a closed-loop gas circuit and gas cleaning in the apparatus.

A possible design of the film bioreactor [13–15] is presented in Fig. 1. Four heat transfer zones can be distinguished in the apparatus. These are a liquid film saturation chamber (I), a mechanically stirred chamber (II), a liquid inlet chamber (III), and a flow circuit (IV). Only when the necessary concentration of the gaseous substrate dissolved in the liquid and the necessary temperature are ensured in each of these zones can a high product output capacity be attained. Fluid dynamics and mass transfer in the mechanically stirred chamber II have been comprehensively investigated to date, while mass transfer in the falling liquid film in chamber I needs to be further analyzed.

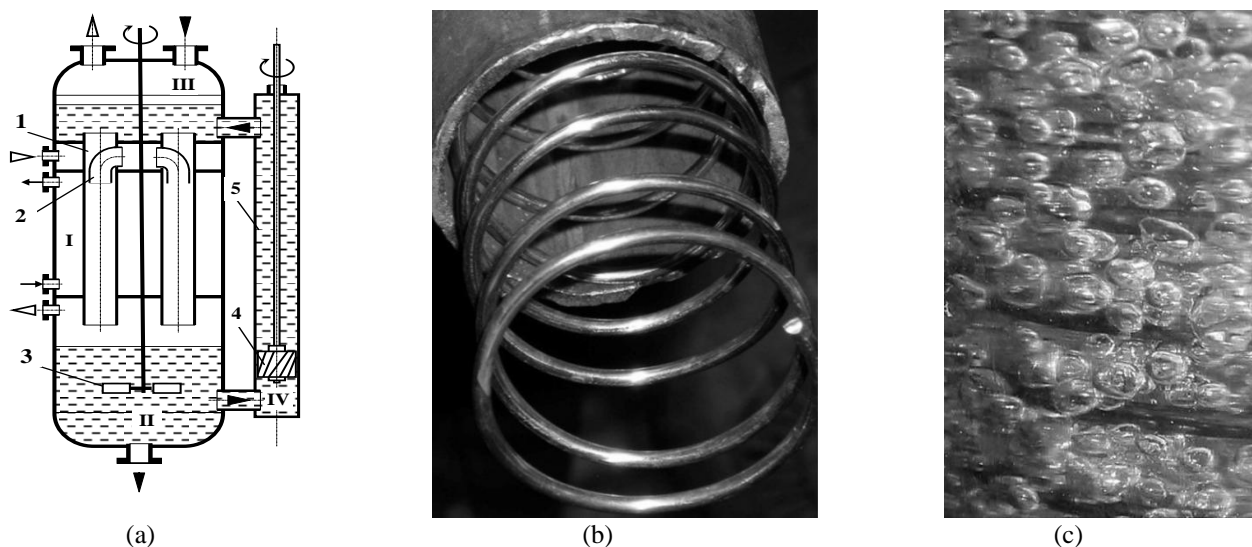


**Fig. 1.** Film bioreactor: (a) reactor design, (b) contact device, and (c) gas bubbles in the falling liquid film; (1) tube of the contact device, (2) gas pipe, (3) stirrer, (4) pump, and (5) circulation pipe.

### DATA SYSTEMATIZATION

Here, we present an analysis of results obtained by N.A. Voinov and his colleagues in their research and development works on film bioreactors. The methods of acquisition and processing of hydrodynamic and heat and mass transfer data for turbulent falling films are described elsewhere [16, 17]. Experiments were carried out on *Candida scottii* yeast and on hydrogen bacteria *Ralstonia eutropha* [18–20].

#### Fluid dynamics in the film saturation chamber.

The highest heat and mass transfer efficiency and the highest liquid throughput capacity are achieved with contact devices whose surface has large-scale artificial helical-rib roughness made from a wire or ribbon [10] (Fig. 1b). In this case, part of the liquid, flowing between roughness coils, is set in combined rotational and translational motion, which favors its uniform distribution along the contact device perimeter without separation and formation of jet flows even on fouled and tilted film-forming surfaces.

The optimum height of the ribs of the helical roughness (wire diameter or ribbon width) is  $h = 3-5 \text{ mm}$  [21]. As the rib height is further increased, there is no significant increase in the saturation intensity because of

decrease in the phase contact area. The maximum possible rate of liquid flow through the contact device at its diameter of 45–100 mm and  $h = 3-4 \text{ mm}$  can be estimated using the relationship

$$G = 1,2 \exp(0,04 \cdot d), \quad (1)$$

where  $G$  is the highest liquid flow rate allowing film flow ( $\text{m}^3/\text{h}$ ) and  $d$  is the inner diameter of the contact device tube (mm).

For example, at a contact device diameter of 48 mm, the liquid flow rate ensuring the formation of an annular falling film is 2 to 8  $\text{m}^3/\text{h}$ . At a lower liquid flow rate, the surface is incompletely wetted; at a higher flow rate, there will be a decrease in the phase contact area. An important design feature of the contact device is that the upper coils of the roughness helix should be placed in the annular gap between the gas pipe and the tube surface in order to set the liquid in rotational and translational motion and to prevent its breaking away from the rib edges upon its running on the roughness ribs.

Contact devices may be made from ribbon coils with a deflected side edge [10] or from a porous body [15]. In the former case, the metal consumption is reduced; in

the latter case, the saturation of the liquid with the gaseous substrate is markedly intensified.

The thickness of the gas-liquid film flowing down the surface of a contact device with helical roughness is several times larger than the thickness of the film on a hydraulically smooth wall and can reach a value of 25 mm or above [22, 23] (Fig. 2). The liquid flow in the former case is stable in a wide range of flow rates (Reynolds number  $Re = 4G/\nu\pi d = 20\,000\text{--}100\,000$ , where  $G$  is the liquid flow rate ( $\text{m}^3/\text{s}$ ) and  $\nu$  is the kinematic viscosity of the yeast suspension ( $\text{m}^2/\text{s}$ ).

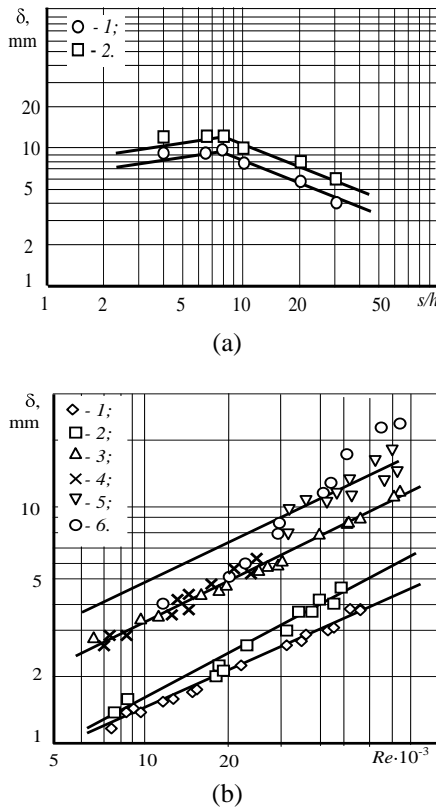


**Fig. 2.** Thickness of the falling liquid film as a function of the (a) roughness parameter and (b) Reynolds number at  $d = 51$  mm,  $\nu = 1 \cdot 10^{-6} \text{ m}^2/\text{s}$ , and a contact device tube length of  $l = 1.6$  m. (a)  $h = 5.5$  mm;  $Re = (1)$  30 000 and (2) 45 000. (b)  $s/h = 8$ ; (1, 2) film flowing down the outer surface of the contact device tube,  $h = 0$ ; (3–7) film flowing down the inner surface,  $h = (3)$  1.85, (4) 3.0, (5) 5.5, and (6) 6.0 mm.

Experiments demonstrated that, as the roughness rib height and the dynamic viscosity of the yeast suspension are increased, the falling liquid film on the contact device surface becomes thicker. The largest thickness value is observed at a roughness parameter of  $s/h = 4\text{--}8$  (Fig. 2a), where  $s$  is the roughness coil spacing. Surfactants do not exert any significant effect on the thickness of the liquid film.

The thickness of the gas-liquid film increases with the distance traveled by the film and becomes constant

at  $l \approx 1.6$  m. It is suggested that the liquid film thickness in the valley of the helical roughness,  $\delta_v$  (Fig. 3), be calculated using the following relationship [10]:

$$\delta \left( 1 \pm \frac{\delta}{2R} \right) = \left( 1 \pm \frac{h}{2R} \right) \frac{hs}{s+e} + \left\{ \frac{\delta^2}{\rho^2 g} \left[ \frac{\lambda e}{8 s+e} + \frac{s}{4 \pi^{1/2} \sigma_1 s+e} \right] \right\}^{1/3}, \quad (2)$$

where  $\rho$  is the density of the gas-liquid mixture ( $\text{kg}/\text{m}^3$ ),  $e$  is the width of a roughness rib (m),  $\lambda$  is the friction factor of the liquid film on the smooth wall of the tube,  $\Gamma = G/\pi d$  is the mass irrigation density ( $\text{kg}/(\text{s m})$ ),  $R$  is the tube radius (m),  $\sigma_1 = 8$  is an empirical correction, the sign “+” refers to a film flowing down the outer surface of the tube, and the sign “-” refers to a film flowing down the inner surface of the tube.

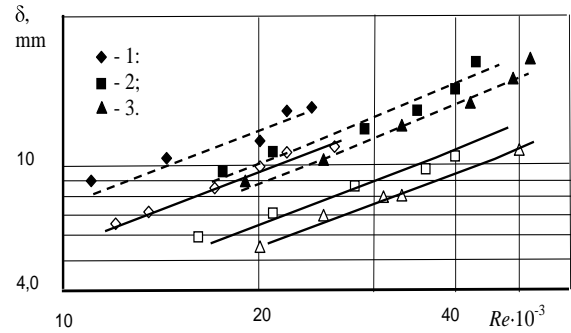


**Fig. 3.** Thickness of the yeast suspension film versus Reynolds number at  $d = 51$  mm,  $s/h = 6$ , and  $h = 3$  mm. Experimental data points:  $\nu = (1)$   $1.2 \cdot 10^{-6}$ , (2)  $0.66 \cdot 10^{-6}$ , and (3)  $0.55 \cdot 10^{-6} \text{ m}^2/\text{s}$ . The solid and dashed lines represent data pertaining to roughness valleys and roughness ribs, respectively.

The density of the gas-liquid mixture in Eq. (2) is given by

$$\rho = \rho_l(1 - \varphi) + \rho_g \varphi,$$

where  $\varphi$  is the gas content and  $\rho_g$  and  $\rho_l$  are the gas and liquid densities.

The friction factor is calculated using Eq. (3) and experimental data (Fig. 4) [10]:

$$\lambda_r = \frac{8\rho^2 g h^3}{\Gamma^2} \left\{ \left( 1 \pm \frac{h}{2R} \right) \frac{s}{s+e} + \frac{\Gamma^{2/3}}{h\rho^{2/3} g^{1/3}} \left( 1 \pm \frac{h}{2R} \right)^{1/3} \times \left[ \frac{\lambda e}{8 s+e} + \frac{s}{4\sqrt{\pi}\sigma s+e} \right]^{1/3} \right\}, \quad (3)$$

The kinematic viscosity of the *Candida scottii* yeast suspension as a function of the biomass concentration ( $x = 10\text{--}100 \text{ kg}/\text{m}^3$  at  $38^\circ\text{C}$ ) was calculated as follows [10]:

$$\nu = 7.397 \cdot 10^{-7} + 2.113 \cdot 10^{-8} x, \quad (4)$$

where  $x$  is the microorganism concentration ( $\text{kg}/\text{m}^3$ ).

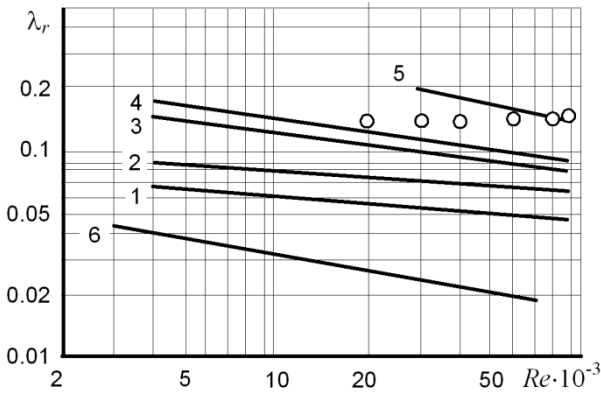


**Fig. 4.** Friction factor versus Reynolds number for a liquid film flowing down the tube surface at  $d = 30$  mm,  $l = 2.5$  m,  $s/h = 10$ , and  $\nu = 1 \times 10^{-6}$  m<sup>2</sup>/s. The lines represent the data calculated via Eq. (3) at  $h = (1)$  0.1 (2) 0.18, (3) = 0.33, (4) 0.45, and (5) 1.0 mm; (6) data calculated using the  $\lambda = 0.3164/Re^{0.25}$  equation. The points represent experimental data [24].

When the microorganism concentration in the culture liquid is above 100 kg/m<sup>3</sup> the kinematic viscosity increases dramatically because of the structuring of the suspension, confirming the existence of an upper limit for the Newtonian flow of suspensions.

The kinematic viscosity of the yeast suspension at a culturing temperature of 30°C is given by the relationship

$$\nu = 0.0197x + 0.793 \cdot 10^{-6}. \quad (5)$$

The density of the yeast suspension at 30°C and  $x = 100$  kg/m<sup>3</sup> is 1025 kg/m<sup>3</sup>, and that at  $x = 200$  kg/m<sup>3</sup> is 1065 kg/m<sup>3</sup>. The dependence of the density of the medium on the bacterial biomass concentration under the biosynthesis conditions can be represented as  $\rho = 995.6 \exp(0.0002 \cdot x)$ .

As the culture liquid flows down the surface with large-scale helical roughness, gas bubbles nucleate in roughness valleys (Fig. 1c), and this leads to the formation of a gas–liquid mixture. This gas bubble nucleation is due to boundary layer separation taking place when the liquid flows from roughness ribs, which generates circulation vortices in the valleys [25]. Once a certain static pressure drop between the vortex and the liquid film surface is reached, which depends on the surface tension and thickness of the film, the gas penetrates into the hollow of the vortex, and this causes the formation of gas bubbles and their buildup in the liquid.

With the optimal arrangement of the coils of the helical roughness, i.e., at  $s/h = 4-8$ , the roughness valleys are filled with gas bubbles to the greatest extent and the bubble diameter is comparable to the height of the roughness rib and is 1.5–4 mm. The gas content of the liquid increases as the height of the rib of the regular helical roughness is increased to  $h = 3$  mm and then remains constant,  $\phi = 0.45$ . The increase in the gas content as a result of an increasing roughness rib height is due to the change in the vortex scale. The interfacial area of the liquid film flowing down the helix-roughened

surface was 700–1000 m<sup>2</sup>/m<sup>3</sup>, while the interfacial area in apparatuses with a turbine-type agitator at its specific power of 0.5–4 kW/m<sup>3</sup> is much smaller [1, 26, 27] and is  $a = 75-200$  m<sup>2</sup>/m<sup>3</sup>.

**Heat and mass transfer in the film saturation chamber.** Mass transfer in a turbulent liquid film has been the subject of numerous works, including studies dealing with contact devices with a rough surface [28–30].

Figure 5 plots the effective mass transfer coefficient in the falling liquid film versus Re as calculated without taking into account the surface area of the gas bubbles. It was established that the highest saturation efficiency is attained at a roughness parameter of  $s/h = 4-8$ .

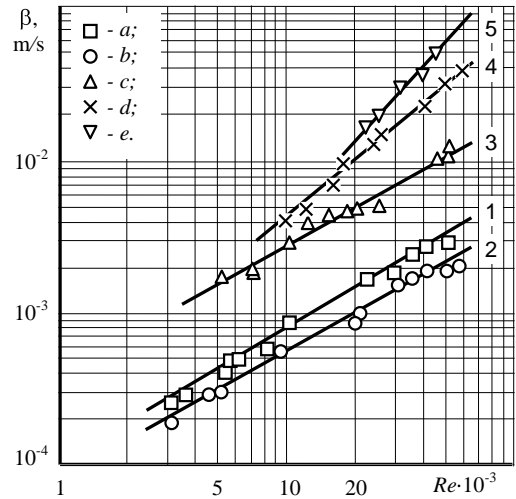


**Fig. 5.** Effective mass transfer coefficient versus Reynolds number for a water film flowing down (lines 1, 2) smooth and (lines 3–5) rough vertical tube surfaces at  $t = 20^\circ\text{C}$ . Experimental data points: (a) inner surface ( $d = 27$  mm,  $l = 2$  m); (b) outer surface ( $d = 30$  mm,  $l = 2$  m); (c–e) internal surface ( $d = 51$  mm,  $l = 1.6$  m,  $s/h = 10$ ),  $h = (c)$  1.85, (d) 3.0, and (e) 5.0 m.

At a dimensionless roughness rib height of , the effective mass transfer coefficient can be calculated using the following relationship [29]:

$$Sh^* = 6.45 \cdot 10^{-4} (Re^*)^{1.505} Sc^{0.5}, \quad (6)$$

for  $h^+ = 150 - 1600$ ,

$$Sh^* = 6.45 \cdot 10^{-4} (Re^*)^{1.505} Sc^{0.5} \left( \frac{h^+}{150} \right), \quad (7)$$

Here,  $Re^* = 4\delta u^*/\nu$ ,  $Sh^* = \beta\delta/D_1$ , and  $Sc = \nu/D_1$ .

The “dynamic” liquid velocity on the rough wall of the tube for a film flowing by gravity is calculated via the formula

$$u^* = \left( \frac{\lambda_r}{8} \right)^{0.5} \frac{\Gamma}{\rho \delta}, \quad (8)$$

where  $\lambda_r$  is the friction factor for the liquid (Fig. 4).

Because of the high gas bubble content of the film, mass transfer should be considered both as contact be-

tween the gas and the surface of the falling film and as interaction between the gas bubbles and the liquid. With this approach, the coefficient of mass transfer between the bubbles of the gaseous substrate and the liquid is  $(0.8-2) \cdot 10^{-3}$  m/s and mass transfer coefficient in the liquid film bulk is  $(2-8) \cdot 10^{-3}$  m/s.

Aeration of a falling liquid film through the porous surface of a tubular insert makes it possible to intensify liquid saturation with the gas by a factor of up to 2 [10]. The presence of a surfactant in the fermentation medium reduces the mass transfer coefficient [31] (Fig. 6).

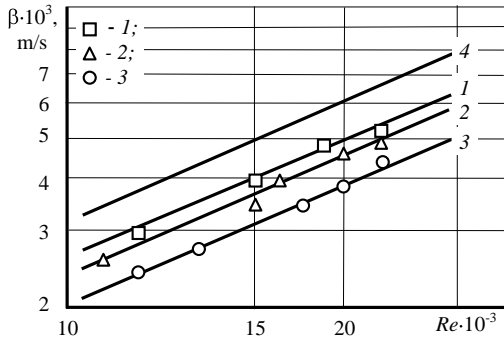


**Fig. 6.** Mass transfer coefficient versus Reynolds number for the gravity flow of a fermentation medium film along the tube surface with helical roughness at  $d = 51$  mm,  $l = 1.24$  m,  $h = 2$  mm, and  $s/h = 8$ . (1-3) experimental data points:  $\sigma = (1) 52 \cdot 10^{-3}$ , (2)  $42 \cdot 10^{-3}$ , and (3)  $34 \cdot 10^{-3}$  N/m. (4) Experimental data for distilled water.

The surface tension values measured for the fermentation medium are plotted in Fig. 7. There are two characteristic regions of the reducing substance (S) concentration effect on the surface tension  $\sigma$ . The surface tension of the fermentation medium is much higher than the surface tension of the culture liquid.

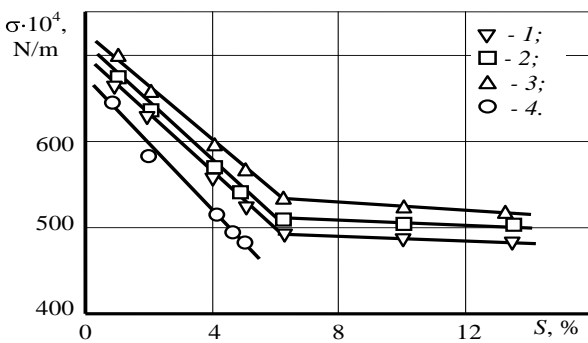


**Fig. 7.** Surface tension of the fermentation medium versus the concentration of reducing substances of molasses. (1-4) Experimental data points:  $t = (1) 45$ , (2) 30, and (3)  $10^\circ\text{C}$ ; (4) hydrolysate from wheat grains at  $t = 20^\circ\text{C}$ .

The surface tension of a bacterial suspension grown in Schlegel's medium is

$$\sigma = (74-79) \cdot 10^{-3} \text{ N/m in the concentration range } x = 1-80 \text{ kg/m}^3 \text{ at } 30^\circ\text{C}.$$

As water evaporates from the surface of the falling liquid film during culturing, the equilibrium gas concen-

tration decreases according to the following relationships because of the change of the partial pressure at the interface [31] (Fig. 8):

for the smooth surface of the contact device tubes,

$$\frac{c_g}{c^*} = \exp(-0.06 \cdot R), \quad (9)$$

for the surface with helical roughness,

$$\frac{c_g}{c^*} = \exp(-0.014 \cdot R), \quad (10)$$

Here,  $c^*$  is the equilibrium oxygen concentration when there is no vapor outflow,  $c_g$  is the equilibrium oxygen concentration in the case of vapor outflow taking place, and  $R$  is the specific water vapor flow rate ( $\text{kg}/(\text{m}^2 \cdot \text{h})$ ).

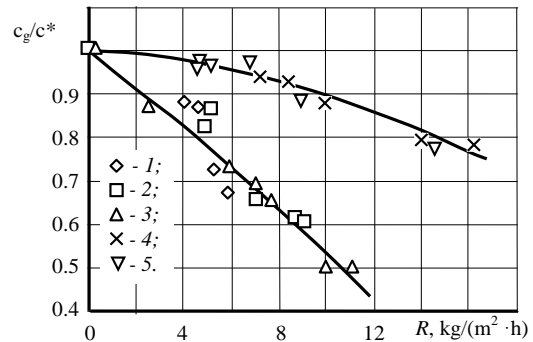


**Fig. 8.** Ratio of the oxygen concentrations in the liquid at the interface versus the specific flow rate of evaporated water for the liquid film flowing downwards by gravity. Experimental data points: (1-3) smooth tube surface,  $t_g = 25^\circ\text{C}$ ,  $t_l = (1) 40$ , (2) 50, and (3)  $60^\circ\text{C}$ ; (4, 5) rough surface,  $t_g = 25^\circ\text{C}$ ,  $t_l = (4) 50$  and (5)  $40^\circ\text{C}$ .

Measurements demonstrated that the solubility of oxygen in the fermentation media used is approximately 10% lower than in distilled water.

The presence of microorganisms showing a certain respiratory activity in the liquid reduces the concentration of dissolved oxygen in the falling liquid film at the outlet of the contact device, and it is necessary to take into consideration this circumstance when designing a bioreactor.

Under the assumption that the contact device (zone I in Fig. 1a) is a plug flow reactor, the mass balance equation for the dissolved gas concentration  $C$  in the falling culture liquid film with thickness  $\delta$  can be written as

$$u\delta \frac{dc}{dl} = \beta(c^* - c) - qx\delta, \quad (11)$$

where  $u$  is the mean velocity of the liquid film (m/s),  $l$  is the tube length (m),  $x$  is the yeast concentration in the liquid ( $\text{kg}/\text{m}^3$ ),  $q$  is the respiratory activity of the yeast ( $\text{kg}/(\text{kg s})$ ),  $c^*$  is the equilibrium gas concentration in the liquid ( $\text{kg}/\text{m}^3$ ), and  $\beta$  is the surface mass transfer coefficient (m/s).

At a constant gas partial pressure in the contact zone, we will then obtain

$$c = c^* - \frac{qx\delta}{\beta} + \left( \frac{qx\delta}{\beta} + c_0 - c^* \right) \exp\left(-\frac{\beta l}{u\delta}\right), \quad (12)$$

where  $c_0$  is the concentration of dissolved gas in the liquid at the chamber inlet ( $\text{kg}/\text{m}^3$ ).

Equation (12) provides means to calculate the dissolved gas concentration in the liquid flowing downwards along the tubular insert. According to the data obtained (Fig. 9), the highest intensity of oxygen supply to the culture liquid is observed at a length of 1.5–2.5 m along the tube. As the microorganism concentration in the liquid is increased, the amount of oxygen in the film at the outlet decreases. At  $x = 100 \text{ kg}/\text{m}^3$  (Fig. 9), the oxygen concentration in the liquid film practically does not increase; that is, the rate of oxygen supply to the liquid is equal to the rate of oxygen consumption by the microorganisms.

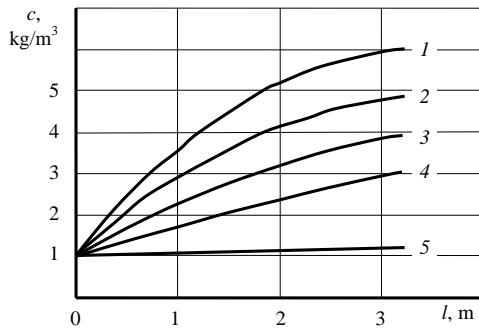


**Fig. 9.** Variation of the oxygen concentration in the yeast suspension film along the length of the tubular insert at  $d = 51 \text{ mm}$ ,  $h = 3 \text{ mm}$ ,  $s/h = 10$ ,  $Re = 50\,000$ ,  $t = 38^\circ\text{C}$ ,  $c^* = 6 \cdot 10^{-3} \text{ kg}/\text{m}^3$ ,  $c_0 = 0.1c^*$ , and  $q = 4.17 \cdot 10^{-5} \text{ kg}/(\text{kg s})$ . The lines represent the data calculated for different yeast biomass concentrations:  $x = (1) 0.1$ , (2) 10, (3) 20, (4) 50, and (5)  $100 \text{ kg}/\text{m}^3$ .

Figure 10 presents the results of investigation of heat transfer in the liquid film flowing down the surface with artificial roughness for various rib heights [32]. The largest value of the heat transfer coefficient is observed at a rib height of 0.13 mm and a dimensionless parameter of  $h^+ > 29$ . The heat transfer coefficient decreases with an increasing rib height because the gas content increases and the heat conductivity decreases according to the relationship

$$\lambda_{mix} = \lambda_l(1 - \varphi) + \lambda_g\varphi, \quad (13)$$

where  $\lambda_{mix}$ ,  $\lambda_l$ , and  $\lambda_g$  are the heat conductivities of the gas-liquid mixture, liquid, and gas, respectively ( $\text{W}/(\text{m K})$ ).

The following equation was suggested for calculating the heat transfer coefficient in a liquid film flowing down a surface with large-scale artificial roughness [32, 33]:

$$Nu^* = \frac{\alpha\delta_v}{\lambda_{mix}} = 1.2 \cdot 10^{-2} Re^{0.8} Pr^{0.6}, \quad (14)$$

where  $Pr = \nu/a$  is the Prandtl number at the temperature of the liquid.

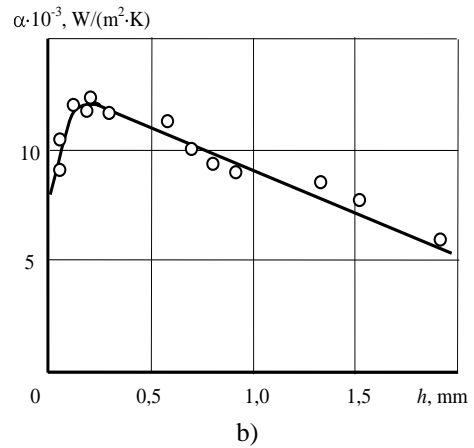
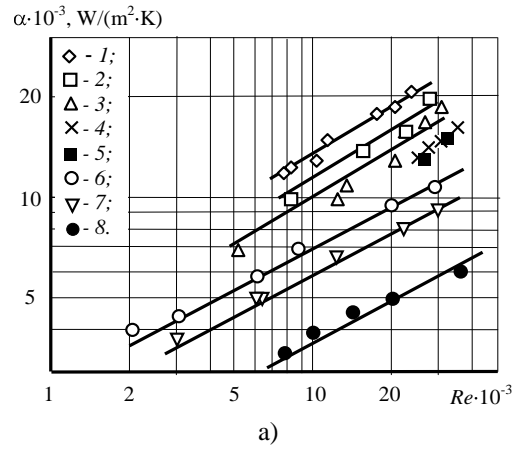


**Fig. 10.** Heat transfer coefficient  $\alpha$  versus (a) the Reynolds number of the liquid flowing by gravity and (b) the rib height of the helical roughness: (a)  $d = 30 \text{ mm}$ ;  $l = 1.9 \text{ m}$ ;  $Pr = 4,5$ ;  $s/h = 10$ ; film on the outer surface of the tube;  $h = (1) 0.13$  (2) 0.3 (3) 0,7, (4) 0.85, (5) 1.0, and (6) 1.5 mm; (7, 8) film on the inner surface of the tube,  $d = 51 \text{ mm}$ ,  $l = 2.3 \text{ m}$ ,  $h = (7) 2.0$  and (8) 3.0 mm; (b)  $d = 30 \text{ mm}$ ,  $s/h = 10$ ,  $Pr = 4-5$ ,  $l = 1.9 \text{ m}$ ,  $Re = 12\,000$ .

**Mass transfer in the mechanically stirred chamber.** When the axial velocity of the yeast suspension in the chamber is 0.008 m/s, the microorganisms are uniformly distributed in the liquid [10]. At a lower velocity, yeast flotation takes place because of the presence of gas bubbles in the bulk of the culture liquid and, therefore, the liquid should be mechanically stirred.

Two mass transfer zones can be distinguished in the working space of the chamber. These are the jet aeration zone and the mechanical stirring zone. As the liquid flows off the contact devices, the resulting jets with the gas entrained by them plunge into the liquid in the chamber. The greatest degree of mass transfer intensification in this case is observed when the jets travel a distance of  $l = 200 \text{ mm}$ . As this distance is further increased, the mass transfer coefficient decreases because the liquid breaks up into drops and, as a consequence, its momentum diminishes. The values of the bulk mass transfer coefficient in jet aeration are plotted in Fig. 11.

The following relationship is suggested for calculating the bulk mass transfer coefficient in jet aeration [10]:

$$\beta_v = 6 \cdot 10^{-8} \cdot \text{Re}_j \text{Sc}^{0.5}, \quad (15)$$

where  $\text{Re}_j = 2\delta u/\nu$  is the Reynolds number and  $\text{Sc}$  is the Schmidt number.

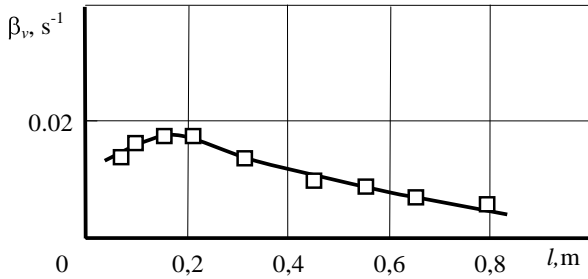


**Fig. 11.** Bulk mass transfer coefficient in the jet aeration of water as a function of the distance traveled by the jet at  $d = 51$  mm,  $t = 20^\circ\text{C}$ , and an outflow velocity of 1.2 m/s.

The height of the jet-aerated zone in the bulk of the culture liquid does not exceed 0.35 m, and its diameter is 0.2 m.

Two hydrodynamic regimes are observed in the mechanically stirred mass transfer zone [26, 34] (Fig. 12). The experimental values of the bulk mass transfer coefficient in apparatuses with a turbine or blade stirrer at  $N(1 - \phi)/V < 10$  in relation to the rotational speed of the stirrer, gas flow rate, and the liquid column height in the chamber [26] are presented in Fig. 12a, and the same data for  $N(1 - \phi)/V > 10$  are plotted in Fig. 12b, where  $N$  is the power spent on stirring (W) and  $V$  is the volume of the chamber ( $\text{m}^3$ ).

The best agreement between the calculated and experimental values of the surface mass transfer coefficient  $\beta$  is provided by the following equation [35]:

$$\beta = 0.33 \left( \frac{nd_{st}d_s}{\nu} \right)^{0.6} \text{Sc}^{\frac{1}{2}} \left( \frac{D_1}{d_s} \right), \quad (16)$$

where  $d_{st}$  is the diameter of the turbine-type stirrer (m),  $d_s$  is the surface-mean diameter (m),  $n$  is the rotational speed of the stirrer ( $\text{s}^{-1}$ ), and  $D_1$  is the diffusion coefficient ( $\text{m}^2/\text{s}$ ).

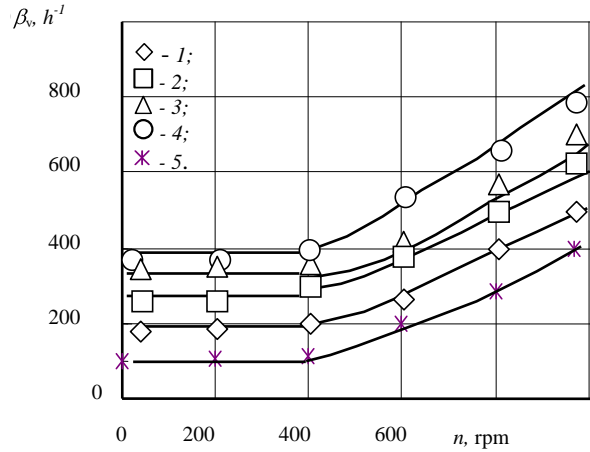
The gain in the mass transfer coefficient achieved by mounting a second turbine-type stirrer on the same shaft was 30% and was due to the further breakup of gas bubbles in the liquid.

The bubble diameter was calculated using the following formula:

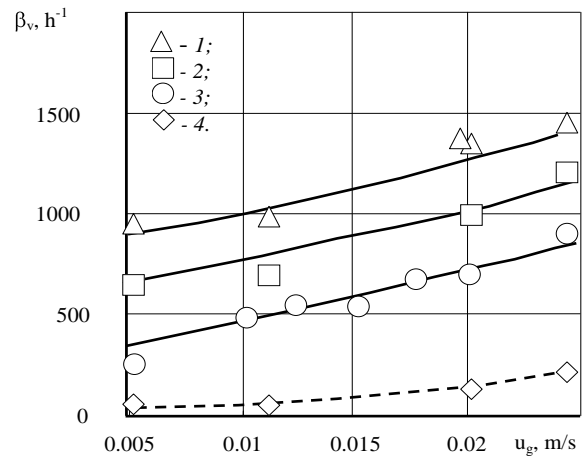
$$d_s = 0.8 \left[ \frac{\sigma^{0.6}}{\left( \frac{N}{V} \right)^{0.4} \rho_1^{0.2}} \right], \quad (17)$$

The mass balance equation for the variation of the dissolved gas concentration  $C$  along the height  $h$  of the aerated layer can be written as

$$u \frac{dc}{dh} = \beta_v (c^* - c) - qx, \quad (18)$$



(a)



(b)

**Fig. 12.** Bulk mass transfer coefficient as a function of (a) the rotational speed of the stirrer and (b) the flow rate average velocity  $u_g$  in the case of a bubbler installed. (a) Blade stirrer, apparatus diameter of  $D = 0.38$  m,  $d_{st} = 0.11$  m; experimental data points: (1)  $u_g = 0.018$  m/s,  $H/D = 1$ ; (2)  $u_g = 0.03$  m/s,  $H/D = 1$ ; (3)  $u_g = 0.04$  m/s,  $H/D = 1$ ; (4)  $u_g = 0.04$  m/s,  $H/D = 0.5$ ; (5) turbine-type stirrer,  $d_{st} = 0.075$  m,  $D = 0.216$  m,  $u_g = 0.01$  m/s,  $H/D = 1$ , where  $H$  is the height of the liquid column. (b) Turbine-type stirrer,  $D = 0.4$  m; experimental data points: (1) two stirrers on one shaft,  $d_{st} = 0.150$  m; (2) one stirrer,  $d_{st} = 150$  mm; (3) one stirrer,  $d_{st} = 80$  mm,  $D = 160$  mm; (4) bubbler without a stirrer.

With the boundary conditions  $h = 0, c(h) = c_{up}$ , we obtain

$$c = c^* - \frac{qx}{\beta_v} + \left( \frac{qx}{\beta_v} + c_{in} - c^* \right) \exp\left( \frac{\beta_v h}{u} \right), \quad (19)$$

where  $c_{in}$  is the gas concentration in the upper layer of the liquid in the bioreactor,  $u$  is the mean velocity of the culture liquid in the working zone,  $\beta_v$  is the bulk mass transfer coefficient ( $\text{s}^{-1}$ ), and  $h$  is the height of the liquid layer in chamber II (m).

Relationship (20) provides means to calculate the gas concentration in the liquid along the height of the aerated layer in the working space of the bioreactor in

the case of microorganisms uniformly distributed in the apparatus (Fig. 13).

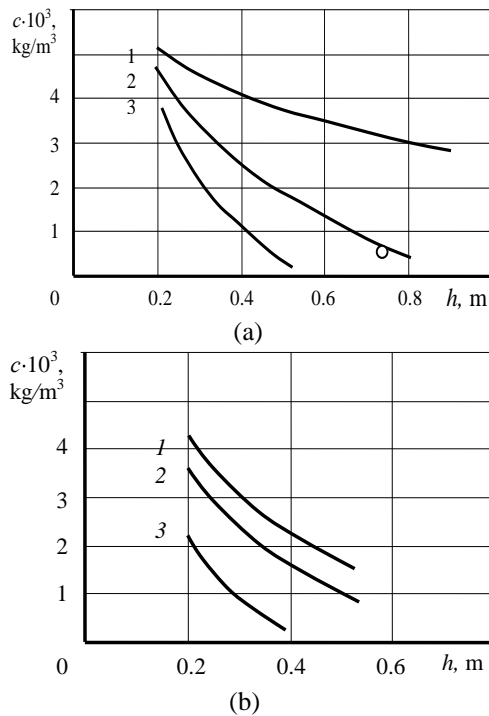


**Fig. 13.** Oxygen concentration profiles along the height of the aerated layer of the culture liquid in the bioreactor: (a)  $u = 0.1$  m/s,  $x = 30.6$  kg/m<sup>3</sup>,  $q = 0.16$  kg/(kg h),  $\beta_v = (1) 0.55, (2) 0.15,$  and  $(3) 0.001$  s<sup>-1</sup>; (b)  $x = 44$  kg/m<sup>3</sup>,  $q = 0.16$  kg O<sub>2</sub>/(kg h),  $\beta_v = 0.15$  s<sup>-1</sup>,  $u = (1) 0.15, (2) 0.1,$  and  $(3) 0.05$  m/s.

**Mass transfer in the flow circuit of the bioreactor.** The variation of the dissolved gas concentration along the length  $l$  of the flow circuit IV and in chamber III can be calculated using the following relationship (20):

$$u \frac{dc}{dl} = -qx, \quad (20)$$

Integration of this relationship subject to the boundary conditions  $l = 0, c = c_c$  yields

$$c = c_c - \frac{qxl}{u}, \quad (21)$$

where  $c_c$  is the gas concentration in the culture liquid at the inlet of the flow circuit.

According to the aforesaid, in the calculation of bioreactor parameters the concentration of dissolved gas in the culture liquid at the outlet of the film flow chamber is determined from relationship (12). The concentration of the dissolved gaseous substrate can be varied both by regulating the liquid flow rate in the flow circuit and, in some case, by regulating the gas phase velocity in the contact devices. The mass transfer coefficient data (Figs. 5, 6) suggest that the concentration of microorganisms in the film saturation chamber (compared to the other zones of the bioreactor) is not limited by

the gas substrate. Conversely, it ensures a dissolved gas reserve that is then consumed in chamber I.

**Table 2.** Calculated characteristics of bioreactors

Characteristic	Airlift $S = 1.5\%$	Film $S = 3\%$	Film $S = 7\%$
Output capacity, t/day	6	6	6
Amount of metal required, t	46.6	20	18
Apparatus diameter and height, m	$7.4 \times 14.2$	$5.5 \times 10$	$3.5 \times 10$
Specific energy input in culturing, kW/kg	1.2	0.8	0.9
Air flow rate, m <sup>3</sup> /h	12 500	0–3000	0–3000
Fresh water flow rate, m <sup>3</sup> /h	44	0	0
Spent liquid (discharge) flow rate, m <sup>3</sup> /h	69.0	12.8	8.2
Electricity consumption, kW h	428	232	200

Calculations demonstrated that, as the concentration of reducing substances in the nutrient wort increases in the  $S = 1$ –10% range at a given output rate, the necessary volume of the bioreactor decreases and the concentration of microorganisms in the culture liquid increases with an insignificant increase in energy consumption for gaseous substrate transport (Fig. 14).

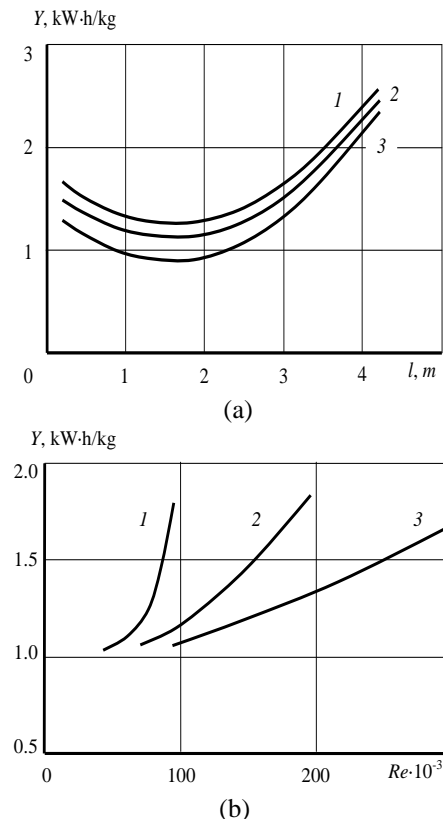


**Fig. 14.** Specific energy consumption versus (a) the contact devices length  $l$  and (b) the Reynolds number of the liquid: (a)  $d = 80$  mm,  $h = 4$  mm,  $s/h = 6$ ,  $Re = 170\,000$ ,  $S = (1) 5, (2) 3,$  and  $(3) 1\%$ ; (b)  $l = 1.5$  m,  $S = 3\%$ ,  $d = (1) 50, (2) 80,$  and  $(3) 100$  mm.

Raising the gas pressure in the bioreactor does not lead to any significant change in the energy consumption in the process. The energy input in gas compression is compensated for by the increase in the equilibrium oxygen concentration in the liquid and by the decrease in the power consumed by the circulation pump. The circulation ratio and, accordingly, energy consumption can be reduced by raising the partial pressure of the saturating gas in the contact zone and by installing several film saturation chambers along the apparatus height. It is clear from the data presented in Table 3 that film bioreactors are capable of processing concentrated media at low gaseous substrate and spent liquid flow rates and high microorganism concentrations. They have moderate dimensions and need a comparatively low energy input for their operation.

The film bioreactor provided a basis for designing culturing processes involving a closed-loop gas circuit and gas purification [36]. This is a step forward in developing environmentally friendly microbiological synthesis technologies that rule out continuous air consumption and gas emission into the atmosphere.

The basic principle of developing an environmentally friendly technology is to organize a closed-loop gas circuit. This principle can be implemented by removing the metabolism products released in the reactor and by returning the purified gas into the reactor after the addition of the necessary amount of the required component. Carbon dioxide released by *Candida scottii* can be efficiently removed from the gas by standard chemical or physical sorption methods. In chemical sorption, the reaction products are neutralized or processed. Physical sorption of carbon dioxide involves regeneration of the sorbent (e.g., 20% monoethanolamine solution) and production of carbon dioxide for the food industry.

The process flowsheet involving a closed-loop gas circuit in oxygen production from atmospheric air by bringing it into contact with a neutral liquid is presented in Fig. 15. Atmospheric air is directed to absorber 4, where it is brought into contact with a neutral liquid having a high oxygen absorption capacity. The oxygen-saturated liquid enters degasser 3, where oxygen is liberated and is then directed to bioreactor 1. The gas containing metabolism products flows from the bioreactor to absorber 2 for cleaning to come into contact with the absorbent. The latter is then directed to the regeneration unit, and the clean gas is returned to the bioreactor. This design rules out contact between atmospheric air and the microorganisms, preventing air pollution. The introduction of an oxygen carrier into the neutral liquid will eliminate the problems associated with oxygen recovery from the culture liquid and will reduce the energy required for liquid circulation.

The setup ensuring a high degree of oxygen recovery from air is schematized in Fig. 16. Here, the goal is achieved by removing carbon dioxide, which hampers microorganism growth, from the culture liquid in degasser 2 followed by gas cleaning in absorber 3. If air is passed through semipermeable membranes in apparatus 4, a decrease in the air flow rate will be achieved owing to the increase in the oxygen concentration in the air. This scheme can be recommended for improving the

existing industrial bioreactors by organizing a closed-loop air circuit. This will markedly reduce the flow rate of the air leaving the apparatus and lower expenditures will be required for its cleaning.

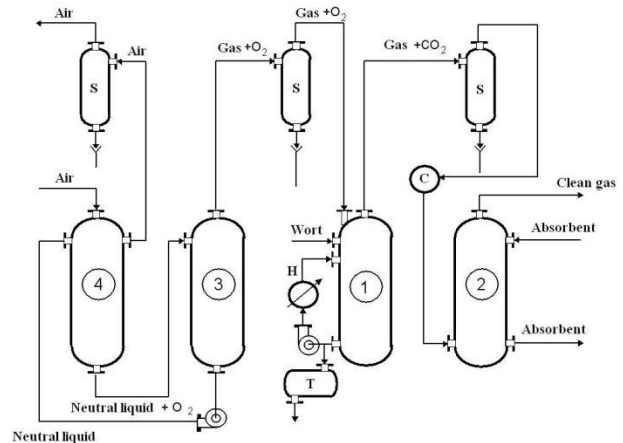


**Fig. 15.** Growth of microorganisms using a neutral liquid: (1) film bioreactor, (2, 4) absorbers, (3) desorber; H = heat exchanger, S = separator, T = tank, C = compressor.

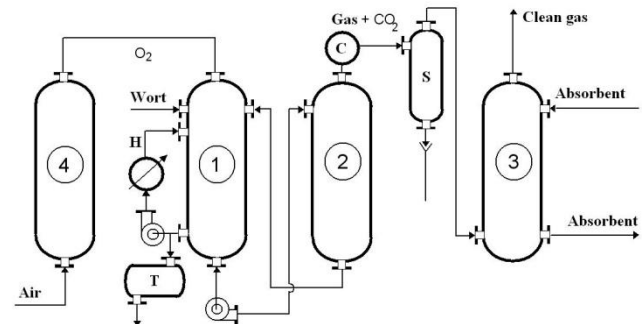


**Fig. 16.** Growth of microorganisms with a high degree of oxygen recovery from air: (1) bioreactor, (2) degasser, (3) absorber, (4) membrane module; H = heat exchanger, S = separator, T = tank, C = compressor.

Of special interest is the combined culturing of microorganisms consuming oxygen and releasing carbon dioxide together with microorganisms consuming carbon dioxide and releasing oxygen [6], for example, simultaneous production of yeast biomass and chlorella, which is usable as a feed additive. The combined technology provides means to organize environmentally friendly, nonwaste manufacturing of microbiological synthesis products that employs a substantially smaller amount of equipment and needing a much smaller capital input and operating expenses.

## CONCLUSIONS

The main advantages of the film bioreactor are that they afford a high biomass concentration in the culture liquid and obviate the need for gaseous substrate transport devices. This makes it possible to organize a closed-loop gas circuit and efficient gas cleaning. The results presented here provide a basis for designing bioreactors.

## REFERENCES

1. Kafarov, V.V., Vinarov, A.Yu., and Gordeev, L.S., *Modelirovanie biokhimicheskikh reaktorov* (Modeling of Biochemical Reactors), Moscow: Lesnaya Promyshlennost', 1979.
2. Henstook, W.H. and Hanratty, T.J., *AIChE Journal*, 1979, vol. 25, no. 1, pp.122–131.
3. Hubbard, G.L., Mills, A.F., and Chung, D.K., *Journal of Heat Transfer*, 1976, vol. 98, pp. 319–320.
4. Hewitt, G. and Hall-Taylor, N., *Annular Two-Phase Flow*, Oxford: Pergamon, 1970.
5. USSR Inventor's Certificate no. 1089117, *Byulleten' izobretenii* (Inventions bulletin), 1984, no 16.
6. USSR Inventor's Certificate no. 1655980, *Byulleten' izobretenii* (Inventions bulletin), 1991, no. 22.
7. USSR Inventor's Certificate no. 1507786, *Byulleten' izobretenii* (Inventions bulletin), 1989, no. 34.
8. USSR Inventor's Certificate no. 1717627, *Byulleten' izobretenii* (Inventions bulletin), 1992, no. 9.
9. USSR Inventor's Certificate no. 1717628, *Byulleten' izobretenii* (Inventions bulletin), 1992, no. 9.
10. Voinov, N.A., Sugak, E.V., Nikolaev, N.A., and Voronin, S.M., *Plenochnye bioreaktory* (Film Bioreactors), Krasnoyarsk: BORGES, 2001.
11. Voinov, N.A., Gurulev, K.V., and Volova, T.G., *Biotechnology in Russia*, 2005, no. 3, pp. 98–107.
12. Voinov, N.A. and Nikolaev, A.N., *Teplos'em pri plenochnom techenii zhidkosti* (Heat Transfer in Liquid Film Flow), Kazan: Otechestvo, 2011.
13. Voinov, N.A. and Nikolaev, N.A., *Plenochnye trubchatye gazo-zhidkostnye reaktory* (Tubular Gas-Liquid Film Reactors), Kazan: Otechestvo, 2008.
14. RF Patent 2012593, *Byulleten' izobretenii* (Inventions bulletin), 1994, no. 9.
15. RF Patent 22211038, *Byulleten' izobretenii* (Inventions bulletin), 2004, no. 1.
16. Nikolaev, A.M., Voinov, N.A., and Nikolaev, N.A., *Theoretical Foundations of Chemical Engineering*, 2001, vol. 35, no. 2, pp. 196–198.
17. Markov, V.A., Voinov, N.A., and Nikolaev, N.A., *Teoreticheskie osnovy khimicheskoi tekhnologii* (Theoretical foundations of chemical engineering), 1990, vol. 24, no. 4, pp. 442–449.
18. Nicolaev N.A., Voinov, N.A., Markov, U.A., *Acta Biotechnologica*, 1991, no. 3, pp. 205–210.
19. Nikolaev, A.N. and Voinov, N.A., *Biotekhnologiya* (Biotechnology), 2009, no. 5, pp. 74–79.
20. Volova, T.G. and Voinov, N.A., *Applied Biochemistry and Microbiology*, 2004, vol. 40, no. 3, pp. 249–252.
21. Voinov, N.A., Nikolaev, A.N., and Voinova, O.N., *Khimiya rastitel'nogo syr'ya* (Vegetable raw materials chemistry), 2009, no. 4, pp. 183–193.
22. Voinov, N.A., Konovalov, N.M., and Nicolaev N.A., *Teoreticheskie osnovy khimicheskoi tekhnologii* (Theoretical foundations of chemical engineering), 1993, no. 6, pp. 638–641.
23. Davies, J.T., *AIChE Journal*, 1972, vol. 18, no. 1, pp. 169–173
24. Hisashi, M., Yasushi, K., Toshiyuki, H., and Tatsuo, N., *Kaganu Kogaku Ronbunshu*, 1991, vol.2, pp. 308–396.
25. Chang, P., *Control of Flow Separation*, Washington, DC: Hemisphere, 1976.
26. Voinov, N.A. and Volova, T.G., *Khimicheskaya promyshlennost'* (Chemical industry), 2007, vol. 84, no. 3, pp. 145–150
27. Keitel, G. and Onken, U., *German Chemical Engineer*, 1981, vol. 4, pp. 250–258.
28. Markov, V.A., Voinov, N.A., and Nikolaev, N.A., *Theoretical Foundations of Chemical Engineering*, 1991, vol. 24, no. 4, pp. 292–298.
29. Konovalov, N.M., Voinov, N.A., Markov, V.A., and Nikolaev, N.A., *Teoreticheskie osnovy khimicheskoi tekhnologii* (Theoretical foundations of chemical engineering), 1993, vol. 27, no. 3, pp. 309–314.
30. Chung L.K. and Mills A.F., *Letters in Heat and Mass Transfer*, 1974, vol. 1, p. 43.
31. Voinov, N.A., Nikolaev, N.A., Eremenko, N.A., and Karpeza, A.G., *Khimiya rastitel'nogo syr'ya* (Vegetable raw materials chemistry), 2006, no. 2, pp. 51–60.
32. Voinov, N.A., Voiova, O.N., and Sugak, E.V., *Thermal Engineering*, 2004, vol. 51, no. 3, pp. 211–215.
33. Voinov, N.A., Zhukova, O.P., and Nikolaev, A.N., *Theoretical Foundations of Chemical Engineering*, 2012, Vol. 46, no. 4, pp. 432–440.
34. Miller, D.N., *AIChE Journal*, 1974, vol. 20, no. 3, pp. 445–453.
35. Strenk, F., *Peremeshivanie i apparaty s meshalkami* (Stirring and Stirred Apparatuses), Leningrad: Khimiya, 1975.
36. Nikolaev, N.A., Voinov, N.A., Markov, V.A., and Gavrilov, A.V., *Biotekhnologiya* (Biotechnology), 1993, no. 3, pp. 23–25.

